Energy Minimization of Carbon Capture and Storage by means of a Novel Process Configuration

Hafiz Ali Muhammad [a,c,ϕ], Haider Sultan [b,c,ϕ], Beomjoon Lee[a], Muhammad Imran[d], Baek Il Hyun [b], Young-Jin Baik[a,c,*],and Sung Chan Nam[b,c, *]

[a] *Thermal Energy Systems Laboratory, Korea Institute of Energy Research, Daejeon 305-343, South Korea*

[b] *Greenhouse Gas Laboratory, Korea Institute of Energy Research, Daejeon 305-343, South Korea*

[c] *University of Science and Technology, Daejeon 305-350, South Korea*

[d] *Mechanical Engineering and Design, School of Engineering and Applied Sciences, Aston University, B4 7ET, Birmingham, UK*

Abstract

Carbon capture and storage is considered a key technology for decarbonizing the heat and power industries and achieving net zero emission targets. However, the significant energy requirements of the process as currently utilized hinders its widespread implementation. This work presents a novel process configuration by which the energy expenditures of carbon capture and storage can be minimized. This configuration is intended to enhance heat integration during the capture process through an innovative combination of three stripper modifications, namely lean vapor compression, a rich solvent split with vapor heat recovery and reboiler condensate heat recovery using a stripper inter-heater in a single flow-sheet. For carbon dioxide compression, a novel pressurization strategy involving carbon dioxide multi-stage compressors, a heat pump system and a supercritical carbon dioxide power cycle was designed and evaluated. The heat pump was used for carbon dioxide liquefaction while the supercritical carbon dioxide power cycle was employed to recover the intercooling heat. Through a comprehensive parametric investigation of the proposed configuration, the optimum value of the key operating parameters i.e., the split fraction, flash pressure, stripper inter-heater location, stripper inter-heater solvent flowrate, carbon dioxide liquefaction pressure and supercritical carbon dioxide cycle turbine pressure ratio were estimated. The performance of the proposed design at the optimized condition was quantified in terms of the reboiler heat duty, the carbon dioxide pressurization power and the equivalent work and compared to a baseline case post-combustion carbon capture and storage process. The proposed case reduced the reboiler heat duty from 3.36 GJ/TonneCO_2 to 2.65 GJ/TonneCO_2 and the electric power required for carbon dioxide compression from 16,691 kW to 14,708 kW. The results demonstrate that the new design can significantly

ϕ Both the authors contributed equally to this work.

* Corresponding Author: Young-Jin Baik (twinjin@kier.re.kr) and Sung Chan Nam (scnam@kier.re.kr)

reduce the reboiler duty, compression power and equivalent work by 21.1%, 11.88%, and 15.8%, respectively.

Keywords: Post-combustion carbon dioxide capture, Novel capture process configuration, Hybrid carbon dioxide pressurization system, Supercritical carbon dioxide power cycle

Nomenclature

a_i	Stoichiometric coefficient of component *i* in reaction equation.
$a^{g,l}$	Area of the gas-liquid interface
BC	Conventional multistage compression established as the baseline case
CCS	Carbon capture and storage
C_i	Concentration of the ith component
C_P	Specific heat capacity at constant pressure (J/kg.K)
dT	Temperature difference
E	Activation energy (Cal/mol)
ENRTL	Electrolyte non-random two-liquid
GA	Genetic algorithm
h	Enthalpy (J/kg)
H	Henry Constant
k	Pre-exponential factor
K	Overall mass transfer coefficient
m	Mass flow rate (kg/s)
M	Rate of mass transfer
MEA	Monoethanolamine
n	Exponent of Temperature, which is zero
N	Number of components in the reaction
ORC	Organic Rankine Cycle
P	Pressure (kPa)
PP	Pinch point in the heat transfer process
Q	Rate of heat transfer (W)
r	Reaction rate.
R	Universal Gas Constant
SH	Refrigerants' degree of superheat at the HP's compressor inlet (K)
s	Entropy (J/kg.K)
T	Temperature (K)
HP	Heat pump
W	Power (W)
X	Quality
State $1CO_2$–$12CO_2$	CO_2 states
State 1Refr–4Refr	Refrigerant R290 states

Greek Symbols

ϕ	Percentage of savings in equivalent work
η	Isentropic efficiency of compressors and pumps
γ	Activity coefficient in liquid phase

Subscripts

BC	Conventional multistage compression established as the baseline case
C	Cooling temperature
Comp	Compressors
Comp2	CO_2 compressor at the end of CCS chain
CW	Cooling water
Eq	Equivalent work
Eva	Evaporator
FG	Flue gas
In	Incoming CO_2
is	Isentropic
o	Ambient conditions
Out	Conditioned CO_2 at the outlet
ORC	Organic Rankine Cycle
PC	Proposed design
R	Ratio
Refr	Refrigerant or HP working fluid
SC	Subcooling
sCO_2	Supercritical CO_2
State $1CO_2$–$12CO_2$	CO_2 states
State 1Refr–4Refr	Refrigerant R290 states
Turb	Turbine

1. Introduction

Carbon capture and storage (CCS) is a key technological measure for reducing the emission of greenhouse gases (GHG) from stationary emission sources such as thermal power plants and ensuring a sustainable and reliable global energy supply. CCS has the potential to significantly reduce carbon dioxide (CO_2) emissions and mitigate climate change [1] and is, therefore, regarded as one of the most important research frontiers for the development of a sustainable future [2]. Different technologies, including oxy-fuel combustion, pre-combustion and post-combustion [3], as well as different materials that are capable of selective sorption of CO_2 (chemical or physical) [4] are available for CO_2 sequestration.

Post-combustion CO_2 capture, making use of an aqueous amine absorption process, is an especially promising technology because it is inherently flexible and can be integrated into various energy systems or

retrofitted into existing facilities [5]. The carbon capture step is followed by CO_2 transportation to the storage site, as shown in Fig. 1. Both of the major steps involved in the CCS process – CO_2 capture and transportation to a storage site – are energy-intensive processes and can produce up to a 14% reduction in net plant efficiency. This significantly high energy penalty hinders the implementation of CCS into power plants [6].

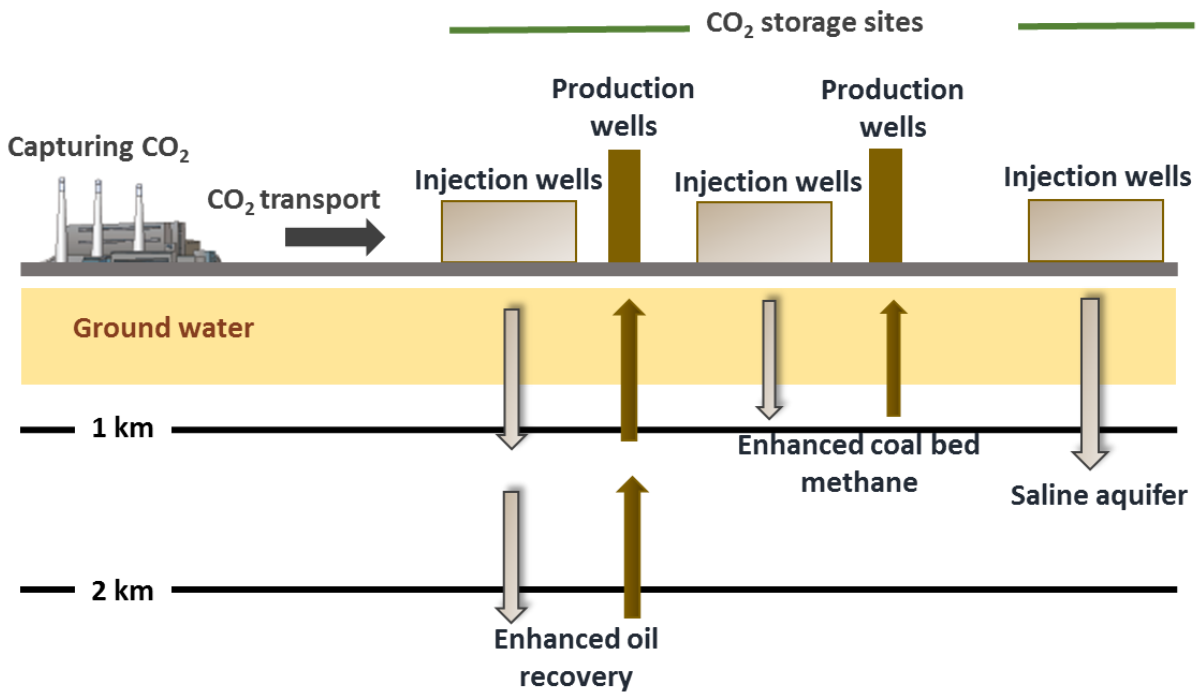

Fig. 1. Carbon capture and storage process.

In the amine absorption process, CO_2 is absorbed at 40-60 °C in an absorber column that makes use of an aqueous amine solvent. This CO_2-rich solvent is then thermally treated at 110-130 °C in a stripper column to produce pure CO_2. The thermal treatment of the CO_2-rich solvent requires a large amount of energy and accounts for approximately 70% of the total process cost [7]. Some researchers have focused on integrating CCS with renewable heat sources such as solar energy in order to provide the energy required for the thermal treatment of the solvent. However, this option remains economically unfeasible, as a large solar field is required to meet the high energy needs of solvent thermal treatment [8]. Therefore, various research activities are aimed at curtailing the energy expenditure of the CCS process by either improving the solvent for the absorption process [9] or the process configuration [10]. Improvement in the process configuration is easier and more effective, because it can be achieved with minimal retrofitting of any existing facility.

Different process configurations such as absorber inter-cooling [10], stripper inter-heating [11], rich solvent splitting [12], stripper overhead compression [13], lean vapor compression (LVC) [14], rich vapor compression [14] and many other process modifications have been reported to reduce the energy penalty of the process. Dmartiz et al. [15] compared the energy consumption of various amine absorption process configurations and concluded that improvement to the configuration has substantial potential to improve the energetic efficiency of the process. Furthermore, the combination of different process configurations has more potential to reduce the energy consumption of the process. A combination of absorber inter-cooling, advanced rich solvent splitting and stripper inter-heating was simulated using ASPEN PLUS^{TM} and resulted in an 18% reduction in reboiler duty [16]. Haider et al. [17] also examined the combination of capture process modifications and achieved 14% reduction in the reboiler duty.

The complete CCS process entails transporting sequestered CO_2 from the capturing facility to the permanent storage site. Pipelines are considered a reliable and efficient mean of CO_2 transportation where the required CO_2 pressure ranges are from 150-200 bar [18]. Therefore, in the first step of the storage process, the pressure of the CO_2 is to be boosted from the captured pressure (1.2-3.5 bar) to the pipeline pressure. The CO_2 pressurization can result in an energy penalty of as high as 12% of the loss of power plant efficiency [19]. Therefore, to curtail this significant energy expenditure, extensive past research has focused on improving the CO_2 compression process. Witkowski et al. [20] investigated a range of compression chain strategies and concluded that the requisite compression power can be reduced by designing a compression chain that makes use of CO_2 liquefaction and pumping. This technique involves compressing the incoming CO_2 from the capture unit to some intermediated liquefaction pressure, after which it is liquefied and then pumped to the target pressure. The liquefaction of CO_2 requires sub-zero condensing temperatures, which makes the use of ambient sink impractical. Therefore, some research activities sought to design refrigeration cycles for CO_2 liquefaction [21]. Alabdulakarem et al. [22] designed a vapor compression cycle (VCC) for CO_2 liquefaction and pumping and explored various refrigerants. They concluded that by complementing the multistage compression with an ammonia-based vapor compression cycle, the power consumption could be reduced by 5.1% compared to conventional multi-stage compression.

The efficiency of the CO_2 compression process can also be improved by recovering compression heat to produce useful work. Romeo et al. [23] optimized the CO_2 compression process by investigating the compression ratio and converting the compression heat of the CO_2 to low-pressure steam in the plant. Meanwhile, Kurtulus et al. [24] integrated an Organic Rankine Cycle (ORC) with CO_2 compressors and conducted a thermodynamic analysis of their system. Pei et al. [25] conducted a similar analysis and concluded that the coupling of an ORC to shockwave-based CO_2 compression is more promising than

simple intercooling compression. Farajollahi et al. [26] studied the impact of integrating an ORC into a 3250 MW thermal power plant with post-combustion CO_2 capture and found out that the efficiency of the plant increased from 31.26% to 33.4% through the application of ORC.

Recently, to reduce the energy expenditure of the CCS process, the integration of fossil-fueled plants with solar hybrid systems has also been aggressively researched. Xu et al. [27] investigated a novel, direct-fired, oxy combustion supercritical CO_2 (sCO_2) power plant integrated with a solar-driven coal gasification array. They found that the proposed design reduced coal consumption by 29.9% and achieved a net energy efficiency of 43.4% with near zero carbon emissions. Similarly, Ghorbani et al. [28] proposed a tri-generation system to produce liquefied natural gas (LNG) and liquefied CO_2 using an adsorption refrigeration system, and desalinated water. Their analysis revealed that hybrid poly-generation systems can enhance the exergetic efficiency of the system up to 88.97%. Although hybrid systems exhibit promising potential to decarbonize the industry for greenfield plants, they lack the capacity to be retrofitted with the existing facility. Therefore, this study sets out to design an advanced CCS process configuration that can be adapted to greenfield plant designs or retrofitted with existing plants to reduce the energy expenditure of the CCS process.

Previous studies demonstrate that extensive research activities have focused on improving the capture process configuration and investigating a liquefaction system design for CO_2 pressurization [29]. However, the majority of these research efforts have addressed these problems separately; therefore, this study aims to remedy this gap by evaluating the entire process chain of CO_2 capture and liquefaction. Recently, Aliyon et al. [30] examined the compete CO_2 capture and liquefaction process; however, their study employed a conventional capture process configuration and ship-based CO_2 transportation. The CO_2 target pressure for their ship-based transportation was 19.7 bar and 26.5 bar, which makes the design of their CO_2 pressurization system significantly differs from pipeline-based transportation.

The originality of this work includes incorporating the complete CCS process while proposing and optimizing a new design for capture, as well as the pressurization process. For the capture process, the combination of stripper modifications has shown improvement potential. Jin et al. [31] reported a 28% reduction in energy consumption by incorporating a combination of stripper modifications, which included an air stripper, flue gas membrane pre-separation, inter-cooler and rich solvent split. However, their study did not consider the auxiliary loads of the added equipment, while the installation of a membrane increases the complexity of the process. In this study, three stripper modifications, namely LVC; a rich solvent split with vapor heat recovery; and heat recovery from reboiler condensate using stripper inter-heater are incorporated into a single flowsheet and auxiliary loads are accounted for while calculating net energy

consumption. For the pressurization process, Muhammad et al. [29] found that integrating liquefaction and pumping into the pressurization system can save the electric power, while Kurtulus et al. [24] demonstrated that the intercooling heat of CO_2 compressors can be recovered to produce power. This study consolidated the effects of liquefaction and pumping and the recovery of intercooling heat by devising a hybrid CO_2 pressurization scheme. The proposed pressurization scheme involves multi-stage compressors, a heat pump (HP) system for CO_2 liquefaction and an sCO_2 power cycle to recover the intercooling heat. Unlike previous studies that investigated ORC to recover the intercooling heat, this study employs an sCO_2 cycle. The sCO_2 cycle offers better efficiency compared to the ORC while harnessing low- to mid-temperature heat sources [32] and integrating the sCO_2 cycle with the proposed CO_2 pressurization scheme does not require any additional working fluid inventory. The capture process configurations were simulated and optimized using ASPEN PLUS^{TM} V10.1 rigorous rate-based modeling, whereas the sCO_2 cycle integrated pressurization scheme was modelled and optimized in the MATLAB environment. The energy expenditure of the proposed capture and pressurization configuration was then calculated at the optimized conditions. The resulting reduction in heat duty and electric power using the proposed design is converted to equivalent work (W_{Eq}) for a fair comparison with the baseline case (BC).

2. Amine-based carbon dioxide capture process description and modelling

The monoethanolamine (MEA) was used as an absorbent during the CO_2 capture process. The liquid phase was modelled using Electrolyte Non-Random Two Liquid (ENRTL) property package while the vapor phase was modelled using the Redlich-Kwong (RK) equation of state. Absorber and stripper columns were simulated using rigorous rate-based models. FLEXIPAC 250Y was used as packing material in the absorber and stripper columns. Absorber and stripper specifications for the CCS process are presented in Table 1. The CO_2 capture process was designed for 90% efficiency at a removal rate of 190 Tonne/hr. The CO_2 capture process was designed for 300 MW coal-based power plants with a designed capacity of 1.5 million tonnes of CO_2 captured per annum. The flue gas composition was set in accordance with the guidelines provided by the Department of Energy (DOE) for the CO_2 capture process. The flue gas molar composition and other specifications are provided in Table 2. These simulation bases were retained throughout the analysis.

Table 1. CO_2 capture process specifications

Component		Specification
Plant type		Coal-based, ~300 [MW]
Absorber	Height	24 [m]
	Diameter	13 [m]
Stripper	Height	11 [m]
	Diameter	8 [m]
Amine flowrate		2900 [Tonne/hr]
CO_2 capture rate (m_{CO2})		190 [Tonne/hr]
CO_2 capture efficiency		90%
CO_2 product purity		99 wt.%

Table 2. Flue gas specifications

Component	Molar composition
CO_2	13 [mole %]
O_2	5 [mole %]
H_2O	10 [mole %]
N_2	72 [mole %]
Pressure (P_{FG})	1.5 [bar]
Temperature (T_{FG})	40 [^oC]
Flowrate (m_{FG})	300 [kg/s]

2.1. Process chemistry

The capture process, essentially a chemical process involving a variety of species and a series of reactions, was modelled using Aspen Plus® [33]. A water, amine and CO_2 mixture were thermodynamically modeled using the ENRTL property package in Aspen Plus® [33]. The chemical reactions taking place in the process were modelled using the power law given in Eq. (1). The reactions and their kinetic parameters; rate constant (k) and activation energy (E) used in Eq. (1), taken from [31], are given in Table 3.

$$r = k(T)^n \, exp\left[\left(\frac{-E}{R}\right)\right] \prod_{i=1}^{N} C_i^{a_i} \tag{1}$$

Table 3. Reaction kinetics

Reactions	Type	Rate constant (k)	Activation energy (E) [Cal/mol]
$H_2O + MEAH^+ \leftrightarrow MEA + H_3O^+$	Equilibrium	-	-
$2H_2O \leftrightarrow H_3O^+ + OH^-$	Equilibrium	-	-
$HCO_3^- + H_2O \leftrightarrow CO_3^{2-} + H_3O^+$	Equilibrium	-	-
$CO_2 + OH^- \leftrightarrow HCO_3^-$	Kinetic	4.32e+13	13249
$HCO_3^- \leftrightarrow CO_2 + OH^-$	Kinetic	2.38e+17	29451
$MEA + CO_2 + H_2O \leftrightarrow MEACOO^- + H_3O^+$	Kinetic	9.77e+10	9855.8
$MEACOO^- + H_3O^+ \leftrightarrow MEA + CO_2 + H_2O$	Kinetic	3.23e+19	156554

2.2. Mass transfer in the carbon dioxide capture process

The mass transfer rate in the gas-liquid interface is expressed by Eq. (2) [34], below. The overall mass transfer coefficient is calculated by Eq. (3) [34].

$$M_i = a^{g,l}N_i = a^{g,l}K_{tot,i}\left(P_i^{eq} - P_i\right) = a^{g,l}K_{tot,i}\left(H_{E,i}\gamma_i c_i - P_i\right) \quad (2)$$

$$\frac{1}{K_{tot,i}} = \frac{RT}{k_i^g} + \frac{H_{E,i}}{k_i^l} \quad (3)$$

The individual coefficients of mass transfer for species "i" are represented by k_i^g and k_i^l in the gas and liquid phases, respectively. Henry's Constant for CO_2 solubility in water is obtained by regressing Vapor Liquid Equilibrium data [35], while that for CO_2 in MEA is obtained from Wang et al. [36]. The non-random two-liquid (NRTL) model's interaction parameters between MEA & water are obtained from Austgen et al. [37]. The NRTL interaction parameters are set to zero between CO_2 and water. The interfacial area ($a^{g,l}$) and mass transfer coefficient in the liquid (k_i^l) and gas $\left(k_i^g\right)$ phases are derived from Bravo et al. [38].

2.3.1 Baseline case: The carbon dioxide capture process

The conventional CO_2 capture process is shown in Fig. 2. The 30 wt.% MEA solvent enters from the top of the absorber column and absorbs $CO_2$from the flue gas emanating from the bottom of the absorber. After the absorption of CO_2, clean gas exits from the top of the absorber. The CO_2-rich solution from the

bottom of the absorber is then pumped to an economizer before regenerating the CO_2-rich solvent in the stripper column. In the stripper column, CO_2 is stripped from the CO_2-rich solvent by heating it in a reboiler. The stripped CO_2, along with the evaporated water vapors, exit from the top of the stripper column and move to the condenser, where they are cooled. The cooled 2-phase mixture is separated in a flash column that sends the condensed water back to the stripper as reflux and the separated CO_2 to the compression unit to increase the pressure up to 150 bar for transportation and storage. The lean solvent from the stripper bottom exchanges heat in the economizer with CO_2-rich solvent and is cooled to 40 ^oC before feeding back into the absorber.

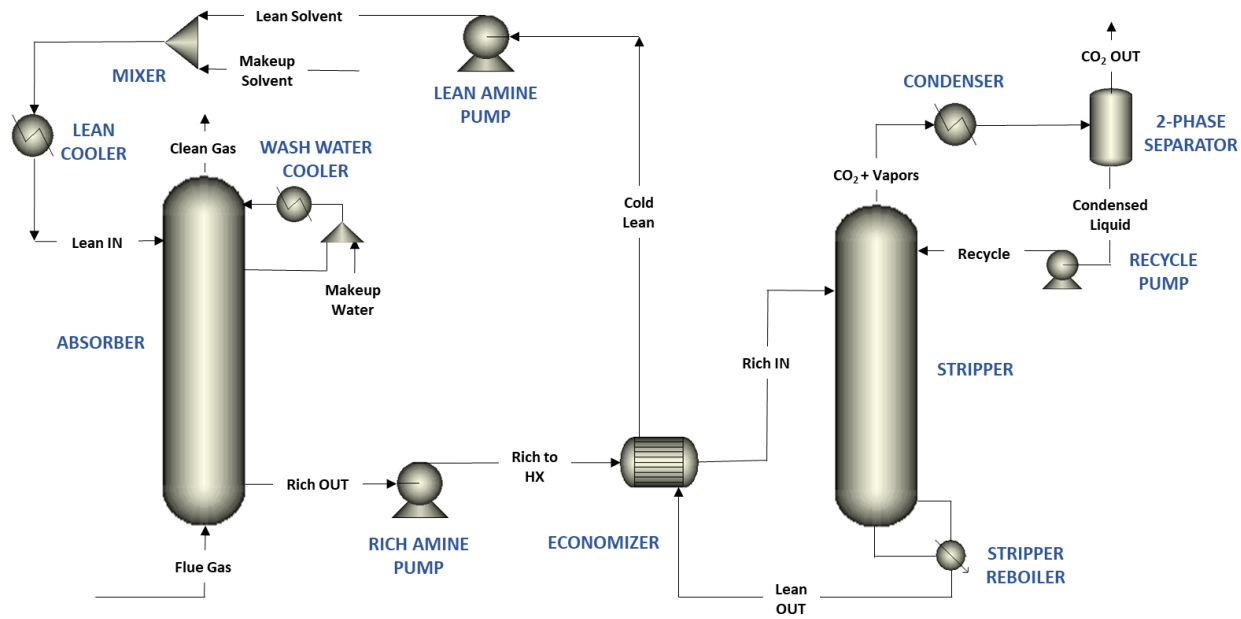

Fig. 2. Baseline case CO_2 capture process flowsheet.

2.3.2. Baseline case for carbon dioxide pressurization

The CO_2 pressurization is an essential step to prepare the captured CO_2 for transportation. Conventionally, the CO_2 is pressurized using multi-stage compression, which is taken as a BC in this study. Each stage of the multi-stage compression comprises a compressor and intercooler, as shown in Fig. 3. The number of stages required depends on the captured CO_2 pressure (P_{In}), target pressure (P_{Out}) and the stage pressure ratio (P_R). The process parameters taken for CO_2 compression are tabulated in Table 4, while the net electric power consumed in the conventional compression process ($W_{Comp,BC}$) is given by Eq. (4).

$$W_{Comp,BC} = \sum_{i=1}^{N} W_{Comp} \quad (4)$$

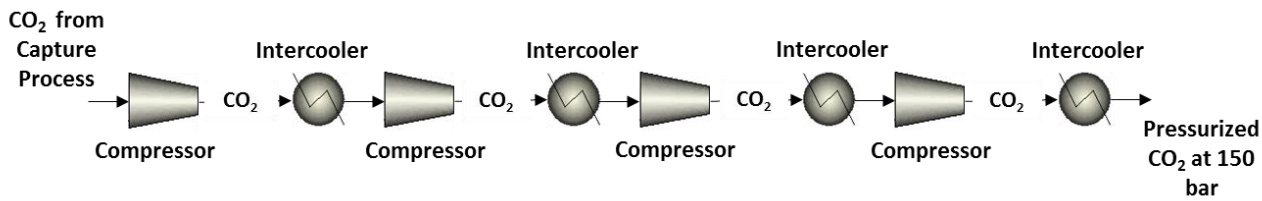

Fig. 3. Baseline case CO_2 compression unit.

Table 4. Performance parameters of CO_2 pressurization during multi-stage compression

Parameters	Values
Compressor and pump isentropic efficiency (η)	0.80
Captured CO_2 pressure (P_{In})	1.9 [bar]
CO_2 target pressure (P_{Out})	150 [bar]
Cooling temperature (T_C)	30 [^oC]
Pinch point (PP)	5
Compressor pressure ratio (P_R) across each stage	3

2.4.1. Proposed carbon dioxide capture process configuration

This proposed novel configuration aims to reduce the heat required for the regeneration of amine solvent by the addition of a HP and integrating process waste heat within the system, as shown in Fig. 4. The CO_2-rich solution stream splits into two sub-streams before entering the economizer. One stream follows the conventional path by entering the economizer and then moving to the stripper column. The other moves to the vapor heat exchanger and recovers heat from the hot CO_2/H_2O vapors mixture exiting the stripper top. This modification (shown with red lines in Fig. 4) will not only reduce the stripper duty, but also the condenser duty by recovering a part of the heat that was being wasted in the condenser. The solvent from the vapor heat exchanger enters the stripper and the H_2O/CO_2 mixture moves to condenser. The stripper column is integrated with a pump-around heater (stripper inter-heater). Some of the solvent from the stripper column is withdrawn and the exchange heat in the stripper inter-heater is then pumped

back to the stripper. Saturated steam at 130 °C is used as the heating utility in the stripper reboiler. The condensate from the reboiler outlet is used as a heating utility in the stripper inter-heater. The modification is marked with violet lines in Fig. 4.

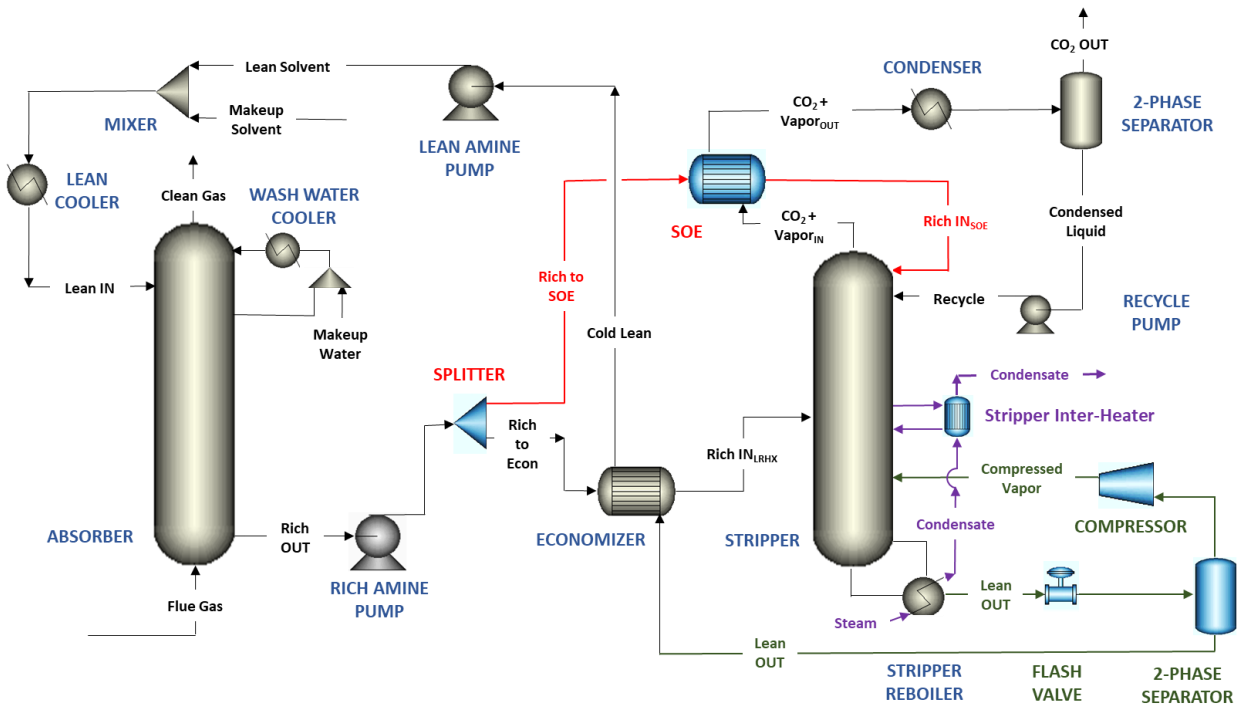

Fig. 4. Proposed CO_2 capture process flowsheet.

A HP was installed to reduce lean loading and add energy to the system. Instead of pumping the CO_2-lean solution from the stripper reboiler into the economizer, it was flashed in a two-phase separator, removing more CO_2 and reducing the lean loading of the CO_2-lean solution. The gas separated in the flash column was compressed back to the stripper pressure and returned to the stripper (as marked with green lines in Fig. 4). The lean solvent from the flash column was pumped to the economizer and further cooled before entering the absorber column. Even though additional electric power is needed to run the added compressor, the reduction in the reboiler's heat duty remains more prominent. For a reasonable comparison, the heat duty and electric power are brought to a common basis in terms of equivalent work, which is discussed later.

2.4.2. Proposed design for the carbon dioxide pressurization process

In the proposed pressurization schematics, the multi-stage compression is assisted by the HP system, as shown in Fig. 5. Increasing the pressure of the liquid CO_2 is significantly less energy-intensive

than gaseous compression. Therefore, the HP is used as a refrigeration cycle to liquefy the CO_2, which is subsequently pumped to the required pressure.

The incoming CO_2 from the capture unit is 1.9 bar, whereas the triple point pressure of CO_2 is 5.17 bar. Therefore, the initial two stages of compression are necessary to raise the CO_2 pressure beyond the triple point pressure. The HP system can thus be installed after either the second or third stages. This study evaluated the performance of the proposed design with HP installed after the second as well as third stage, which is discussed in Section 3.1.5.

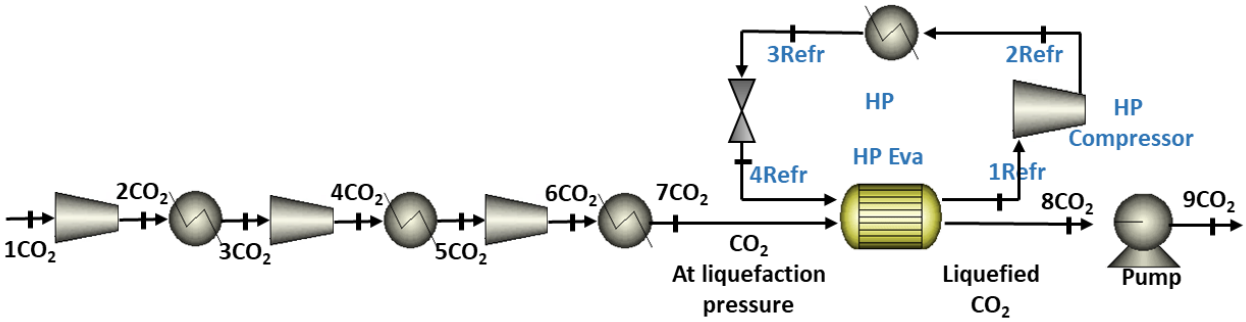

Fig. 5. Proposed heat pump assisted CO_2 compression schematics.

The difference between the conventional and the proposed approach for CO_2 pressurization is elucidated in a P-h diagram in Fig. 6. The baseline approach is multi-stage compression while in the proposed case the last stage is replaced by CO_2 liquefaction and subsequent pumping to the target pressure.

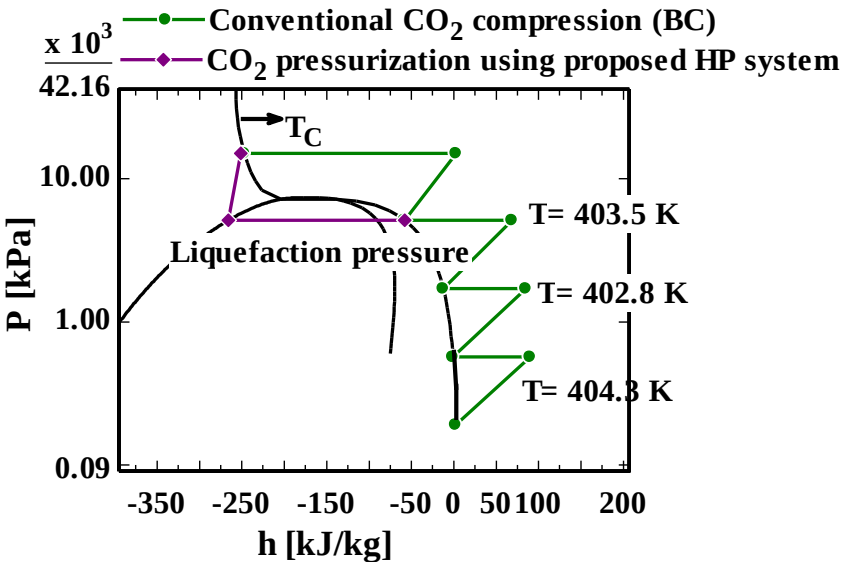

Fig. 6. Thermodynamic routes for CO_2 pressurization.

2.4.3. Modelling framework for proposed carbon dioxide pressurization process

The refrigerant of the HP, which absorbs heat (Q_{Eva}) from the CO_2, is then compressed and adjusted to expel heat into the environment. Propane (R290) is considered as the HP refrigerant in this study. In the evaporator, the saturation parameters of R290 are determined by the pinch point (PP) limit and CO_2 liquefaction temperature. The CO_2 liquefaction temperature is the saturation temperature, corresponding to its liquefaction pressure (P_{7CO2}). State 1Refr in Fig. 5 is determined by identifying the refrigerant's saturation temperature in the evaporator and assuming a degree of superheating (SH) at the HP's compressor inlet. The ambient conditions, which are considered the heat sink for R290, determine the saturation temperature and pressure of R290 in the condenser and, consequently, the State 3Refr. State 2Refr and 4Refr were determined by using a compressor model with isentropic efficiency and assuming isenthalpic expansion.

The calculation procedure of the HP system in the proposed schematics is summarized in Table 5. The discretization scheme is used for the modeling of heat exchangers, details of which can be found in [39]. The net power consumed in the proposed schematics ($W_{Net,PC}$) is given by Eq. (5), where $W_{Comp,CO2}$, W_{Pump} and $W_{Comp,Refr}$ are the power consumed by the initial multi-stage CO_2 compressors, the CO_2 pump and the HP compressor, respectively.

$$W_{Net,PC} = W_{Comp,CO2} + W_{Pump} + W_{Comp,Refr} \quad (5)$$

Table 5. Calculation schematics of the proposed heat pump system

Step	State	Temperature	Pressure	Enthalpy	Comments
1	$7CO_2$	$T_{7CO2} = T_C$	P_{7CO2}	$f(T_{7CO2}, P_{7CO2})$	Using the set values of P_R, T_C, and η_{Comp}; State $7CO_2$ is solved.
2	$8CO_2$	$T_{8CO2} = T_{Sat,8CO2} = f(P_{8CO2})$	$P_{8CO2} = P_{7CO2}$	$f(T_{8CO2}, X=0)$	Calculate Q_{Eva} using heat exchanger model.
3	$9CO_2$	$T_{9CO2} = f(P_{9CO2}, \eta_{Pump})$	P_{9CO2}	$f(T_{9CO2}, P_{9CO2})$	Pump model.
4	1Refr	$T_{1Refr} = f(T_{Sat,4Refr}, SH)$	$P_{1Refr} = P_{Sat,1Refr} = f(T_{4Refr})$	$f(P_{1Refr}, T_{1Refr})$	SH is taken as 5 K.
5	2Refr	$T_{2Refr} = f(P_{Sat,2Refr}, \eta_{Comp})$	$P_{2Refr} = P_{Sat,2Refr} = f(T_{3Refr})$	$f(P_{2Refr}, T_{2Refr})$	Compressor model.
6	3Refr	$T_{3Refr} = T_{Sat,3Refr} = T_C$	$P_{3Refr} = P_{Sat,3Refr}$	$f(T_{Sat,3Refr}, X=0)$	Heat exchanger model.
7	4Refr	$T_{4Refr} = T_{Sat,4Refr} = f(T_{8CO2}, PP)$	$P_{4Refr} = P_{Sat,4Refr} = f(T_{4Refr})$	$f(P_{4Refr}, h_{3Refr})$	Isenthalpic expansion.

2.4.4. Proposed heat pump pressurization process integration with supercritical carbon dioxide cycle

During the multi-stage CO_2 compression, the temperature of the CO_2 at each compressor outlet can reach around 400 K, as is shown in Fig. 6. To make use of this temperature, an innovative scheme of CO_2 liquefaction and pumping integrated with the sCO_2 cycle, as displayed in Fig. 7 is proposed. In contrast to the ORC, the sCO_2 cycle is designed to utilize the intercooling heat, as no additional working fluid is required to operate the sCO_2 cycle. As can be seen in Fig. 7, the heat source and cycle working fluid are both CO_2, and therefore a better temperature match is achieved by employing an sCO_2 cycle. In addition, as the captured CO_2 is liquefied using the HP system, therefore the high-pressure level required to operate an sCO_2 cycle which is generally in the range of 150-250 bar can be attained in an energy-efficient manner by means of the pump. For the integrated design, CO_2 from the State $8CO_2$ is initially pressurized to 200 bar and State $9CO_2$. The high-pressure CO_2 is later divided into three streams, the flowrates of which are given in Fig. 7. The splitting of the total flow is performed in such a way so that the temperature of the

streams after heating at States $10CO_2$, $10CO_2^{/}$ and $10CO_2^{//}$ is comparable. Thereafter, the streams are mixed (State $11CO_2$) and subsequently fed into a turbine to produce electric power.

For the sCO_2 power generation, the turbine power output is W_{Turb} and the power consumed by the compressor to recover the pressure from State $13CO_2$ to $14CO_2$ and complete the process is $W_{Comp2CO2}$. The net power of the sCO_2 cycle is expressed in Eq. (6).

$$W_{Net,Cycle} = W_{Turb} - W_{Comp2,CO2} \tag{6}$$

After the CO_2 has delivered power to the turbine, it is cooled down and subsequently compressed to 150 bar (State $14CO_2$), thereby completing its flow (Fig. 7). After integrating the cycle, the $W_{Net,PC}$ is modified as follow:

$$W_{Net,PC} = W_{Comp,CO2} + W_{Pump} + W_{Comp,Refr} - W_{Net,Cycle} \tag{7}$$

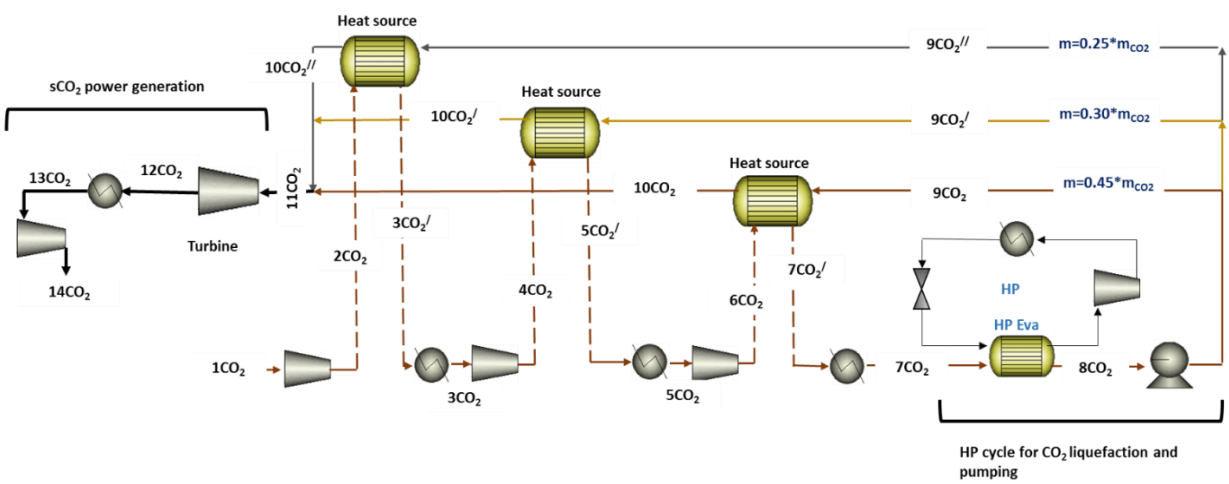

Fig. 7. Heat pump system integrated with a supercritical CO_2 cycle.

2.5. Total equivalent work/performance indicator calculation

In the CCS process, two different energy expenditures are incurred: (i) the electrical power consumed in the pumps and compressors; and (ii) the heat duty in the boiler. For a fair comparison, a common basis for the two types of energy is needed, and therefore W_{Eq} is defined for a performance comparison. The W_{Eq} for the base and the proposed configurations are calculated using Eq. (8):

$$W_{Eq} = \sum \eta_{Turb} * Q_i \left((T_i + 10[K] - T_{Sink})/(T_i + 10[K])\right) + W_{Eelctric} \quad (8)$$

where the turbine efficiency (η_{Turb}) is considered to account for the non-ideal expansion, T_i is the reboiler temperature (K), the temperature of the steam in the reboiler is 10 ^oC higher than T_i, Q_i is the reboiler duty for the base and proposed case (GJ/TonneCO_2) and $W_{Electric}$ is the net electric power consumed during the complete CCS process. All the power entities, electric power and heat, consumed in the base as well as the proposed case, are converted to W_{Eq} using Eq. (8). After calculating the total equivalent work for the base ($W_{Eq,BC}$) and the proposed case ($W_{Eq,PC}$), the net effect (ϕ_{Net}) of the proposed schematics is defined as:

$$\phi_{Net} = (W_{Eq,BC} - W_{Eq,PC})/W_{Eq,BC} \quad (9)$$

The calculation flow chart of the complete CCS configuration proposed is summarized in Fig. 8.

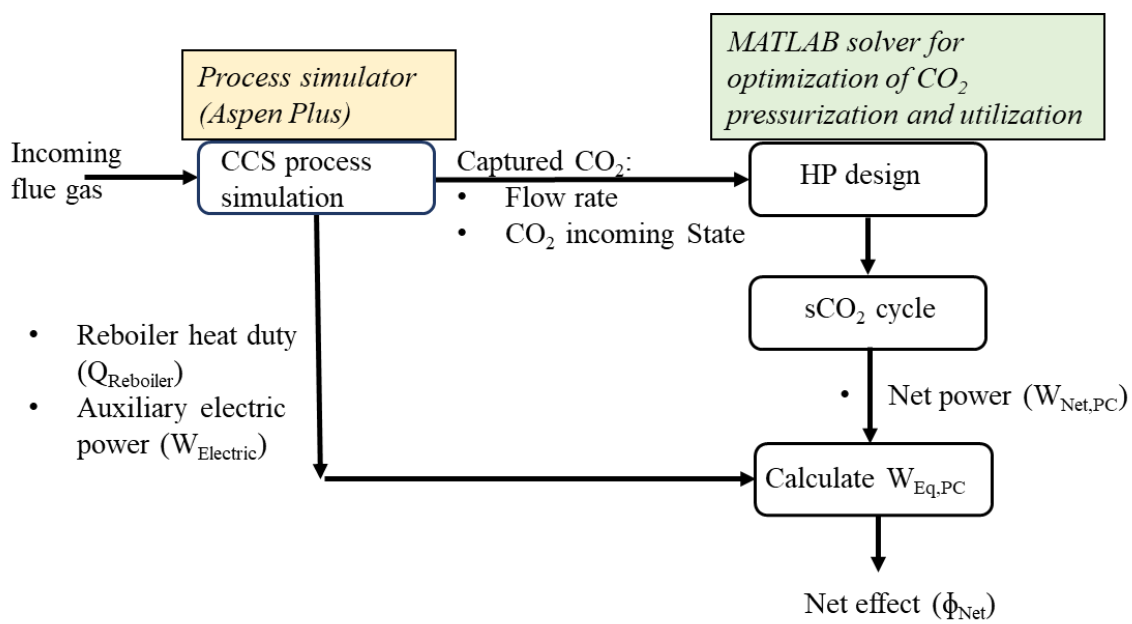

Fig. 8. Calculation flowchart of the proposed carbon capture and storage process configuration.

3. Results and discussion

Initially, the BC was simulated to calculate the reboiler duty, which amounted to 3.36 GJ/TonnesCO_2 for a CO_2 capture rate of 190 TonneCO_2/hr. The four-stage compressors, with a P_R of 3, were established as the BC for CO_2 pressurization. The BC consumes 16691.40 kW of electric power to

increase the pressure of CO_2 from 1.9 to 150 bar. After quantifying the BC, the capture process design is optimized for: split fraction, flash pressure, stripper inter-heater location and stripper inter-heater solvent flowrate. The HP-assisted CO_2 compression integrated with the sCO_2 power cycle is optimized to yield the best performance.

3.1. Split ratio

The CO_2-rich stream is split to enhance the heat integration within the CO_2 capture process. The objective is to recover maximum heat from the top and bottom streams, leaving the stripper. The amount of heat recovered from any of these streams depends on the CO_2-rich solvent flowrate against the respective heat exchanger. The split ratio to the economizer was varied from 0.65 to 0.74 in order to study the effect on the stripper reboiler duty. Fig. 9 shows that 0.67 is the optimum split ratio, which corresponds to the minimum reboiler duty. The split ratio below 0.67 reduces the CO_2-rich solvent flowrate to the economizer and the heat recovered in it. Although heat recovery in the vapor heat exchanger increases due to a higher CO_2-rich solvent flowrate, the sum of the total heat recovery in the economizer and vapor heat exchanger is lower than at the split ratio of 0.67. Similarly, above the 0.67 split ratio, the economizer can recover more heat, but the heat recovery in the vapor heat exchanger declines. The overall impact is the reduction in total heat recovery. The split ratio of 0.67 is the optimum split ratio at which the overall heat recovered in the economizer and vapor heat exchangers is at a maximum and the stripper reboiler duty is minimal.

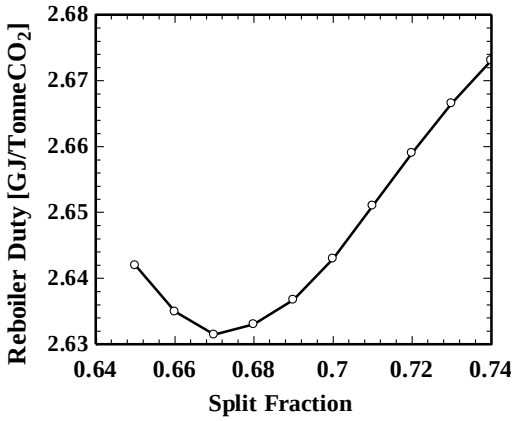

Fig. 9. Reboiler duty variation with split fraction.

3.2. Flash pressure

Lean solvent from the stripper reboiler is flashed in a column to strip out the CO_2, which is compressed back to the stripper pressure. Additional electrical energy is required for the compression of CO_2. The amount of energy required for compression depends on the flashing pressure. However, this additional energy increases the temperature of CO_2 which, upon returning to the stripper, not only adds

energy to the stripper but also acts as a mass and energy stripping agent and reduces the stripper duty. Fig. 10 shows the impact of flash pressure on the compression energy requirement and the stripper reboiler duty. As the reboiler duty is in the form of heat energy and the compressor duty is in the form of electric work, W_{Eq}, is used as the key parameter to determine the optimum flash pressure (Eq. (8)). The impact of the flash pressure on W_{Eq} is shown in Fig. 11, which reveals that 1.3 bar is the optimum flash pressure and corresponds to the minimum total W_{Eq}.

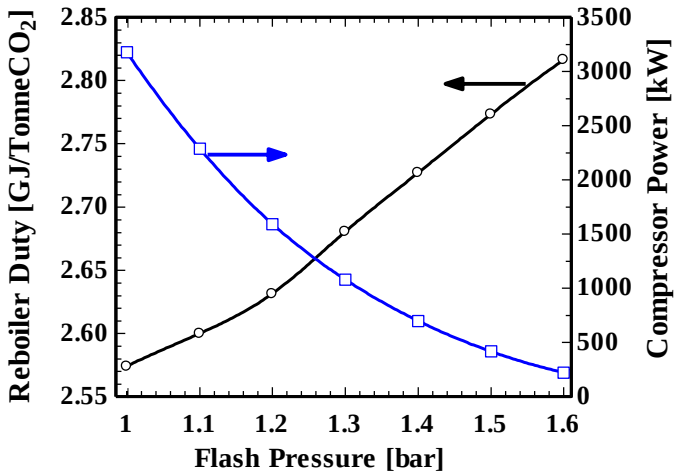

Fig. 10. Effect of the flash pressure on reboiler duty and compressor power.

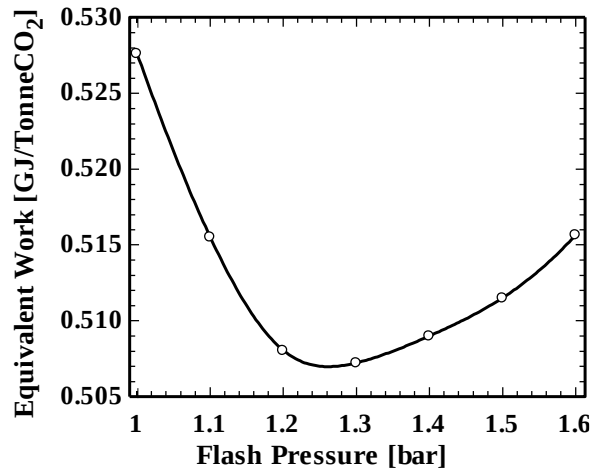

Fig. 11. Effect of the flash pressure on equivalent work.

3.3. Stripper inter-heater location

Saturated steam, used as the reboiler heating utility, exits as condensate at 129 °C. To recover heat from the reboiler condensate, stripper inter-heater is introduced. The stripper has 20 stages. Rich amine is fed from the top (stage 1) while lean solvent leaves from the bottom (stage 20). Amine solvent from a higher stripper stage is withdrawn and heated in a stripper inter-heater using reboiler condensate, and is fed back to a lower stage. To find the optimal withdrawal and feedback location, the withdrawal and feedback stage was varied, and the stripper duty observed.

Fig. 12 shows the impact of withdrawal and feedback stage on the stripper reboiler duty. The liquid at the top stages of the stripper column is at a relatively lower temperature and, therefore, has a high temperature difference from the reboiler condensate and can thus recover more heat. Withdrawal from the lower stage results in a lower temperature difference from the reboiler condensate and, consequently, less heat can be recovered.

As the CO_2-rich solvent is heated in the inter-heater, the CO_2 gas and water vapors begin separating from the solvent. When this vapor-liquid mixture is fed back to a lower stage, the vapor phase interacts

with more liquid coming down and strips more CO_2 from the CO_2-rich solvent, thus reducing the reboiler duty. Stage 2 is the optimum withdrawal location and stage 15 the optimum feedback stage. Feeding below stage 15 does not induce any substantial change in reboiler duty.

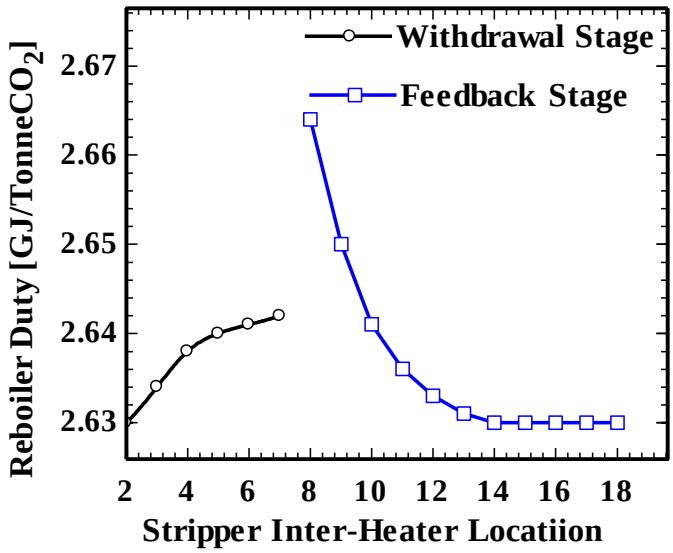

Fig. 12. Stripper inter-heater location optimization.

3.4. Stripper inter-heater flowrate

Hot solvent from the stripper inter-heater, when fed back to the stripper, serves as a stripping agent. The effectiveness of the stripping agent improves at higher temperature and reduces the reboiler duty [40]. Eq. (10) shows that higher temperatures ($\Delta T_{solvent}$) can be achieved by reducing the solvent flowrate ($m_{solvent}$). However, due to the thermal degradation of the solvent, the solvent temperature in the stripper inter-heater should not exceed 120 ^{o}C.

In order to find the optimum flowrate at which the reboiler duty is at a minimum and the solvent temperature is below the degradation temperature (120 ^{o}C), the $m_{solvent}$ to stripper inter-heater was reduced from 3000 kmol/hr to 1000 kmol/hr and its impact on the reboiler duty and solvent outlet temperature was evaluated. Fig. 13 shows that by reducing the inter-heater flowrate, the temperature of the solvent fed back to stripper increases, which also improves the stripping efficiency and reduces the reboiler duty. However, due to the solvent degradation temperature limit, 1750 kmol/hr. is considered the optimum $m_{solvent}$, which corresponds to a stripper inter-heater solvent temperature of below 120 ^{o}C and a lower reboiler duty.

$$Q = m_{solvent} \times c_p \times \Delta T_{solvent} \quad (10)$$

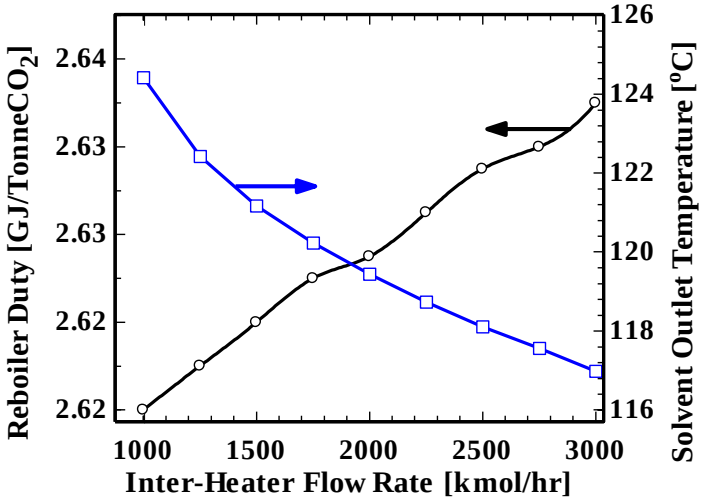

Fig. 13. Effect of stripper inter-heater flowrate on reboiler duty and solvent temperature.

3.5. Optimizing the carbon dioxide pressurization process

The proposed pressurization process aims to reduce the required electric power to raise the CO_2 pressure by replacing one or two stages of CO_2 compressors with an HP system, consequently reducing $W_{Comp,CO2}$. However, due to the application of HP, another source of electric power consumption becomes involved in the form of the compressor of the HP, i.e. $W_{Comp,Refr}$. Therefore, in the proposed design, $W_{Comp,CO2}$ and $W_{Comp,Refr}$ are in a trade-off relationship. Table 6 summarizes the performance of the proposed design with the HP installed after the second and third stage of the compressors. Installing the HP after the third stage of the compressor instead of the second will seemingly increase the $W_{Comp,CO2.}$ However, as can be seen in the table, the $W_{Comp,CO2}$ increases up to 46.49%. At the same time, however, the $W_{Comp,Refr}$ is reduced by 85.80% while the difference in W_{Pump} remains negligible.

Table 6. Performance evaluation with the heat pump installed after the second and the third stages of compressors.

New Design	Liquefaction Pressure [kPa]	CO_2 Multistage Compression ($W_{Comp,CO2}$) [kW]	CO_2 Pump (W_{Pump}) [kW]	HP-Compressor ($W_{Comp,Refr}$) [kW]
2-Stage CO_2 Compressor & HP	P_{5CO2} = 1710	9191.50	1130.70	7581.70

3-Stage CO_2 Compressor & HP	P_{7CO2} = 5130	13465.00	1149.00	1076.60
Percentage change	N/A	+46.49%	-1.62%	-85.80%

The substantial decrease in $W_{Comp,Refr}$ with the HP installed after the third stage is due to the combined reduction in refrigerant flowrate (m_{Refr}) and the P_R across the HP's compressor. Table 7 tabulates the Q_{Eva}, the saturation pressure of the refrigerant in the evaporator and condenser, the resulting P_R and the m_{Refr}. Q_{Eva} decreases and the saturation temperature of the refrigerant in the evaporator increases with the increase in CO_2 liquefaction pressures. Therefore, the m_{Refr} and P_R both decrease, leading to a considerable reduction in $W_{Comp,Refr}$. The subsequent results and discussions are based on HP installed after the third compressor stage.

Table 7. Operating characteristics of the heat pump system installed after the second and the third stages of compressors.

New Design	**Liquefaction Pressure [kPa]**	**Evaporator heat load (Q_{Eva}) [kW]**	**Refr. saturation pressure [kPa]**		**Refr. flow rate (m_{Refr}) [kg/s]**	**P_R across HP's comp**
			Evaporator	Condenser		
2-Stage CO_2 Compressor & HP	P_{5CO2} = 1710	18461.54	171.16	1079.26	68.44	6.30
3-Stage CO_2 Compressor & HP	P_{7CO2} = 5130	10983.51	642.90	1079.26	34.72	1.68
Percentage change	N/A	-40.51%	N/A	N/A	-49.27%	-73.33%

3.6. The integrated supercritical carbon dioxide cycle optimization

Due to the advantages discussed earlier, the compression heat is recovered using an integrated sCO_2 cycle (Fig. 7). For an sCO_2 cycle at a given turbine inlet temperature, an optimum P_R across the turbine is required to maximize the cycle performance [41]. In the analysis, the turbine inlet pressure (P_{11CO2}) is fixed to 200 bar, and hence the turbine outlet pressure (P_{12CO2}) is parametrically investigated in this study. Fig. 14 shows the variation of $W_{Net,Cycle}$ with P_{12CO2}, while the individual variation of W_{Turb} and $W_{Comp2,CO2}$ with

P_{12CO2} is shown in Fig. 15. As can be seen in Fig. 15, the W_{Turb} varies steadily throughout; however, the $W_{Comp2,CO2}$ experienced a sharp decrease at the start, with P_{12CO2}. The sudden reduction of $W_{Comp2,CO2}$ is due to the operation of the compressor near the critical point where the properties of CO_2 substantially vary. Fig. 16 shows the variation of CO_2 density at the compressor inlet with P_{12CO2}. The drastic initial increase in CO_2 density results in a sharp reduction of $W_{Comp2,CO2}$, which causes the sCO_2 power cycle to behave in the manner presented in Fig. 14.

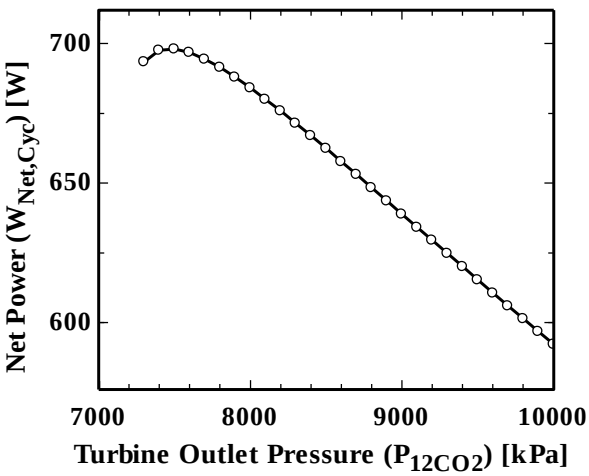

Fig. 14. Supercritical CO_2 power generation ($W_{Net,Cycle}$) variation with turbine outlet pressure (P_{12CO2}).

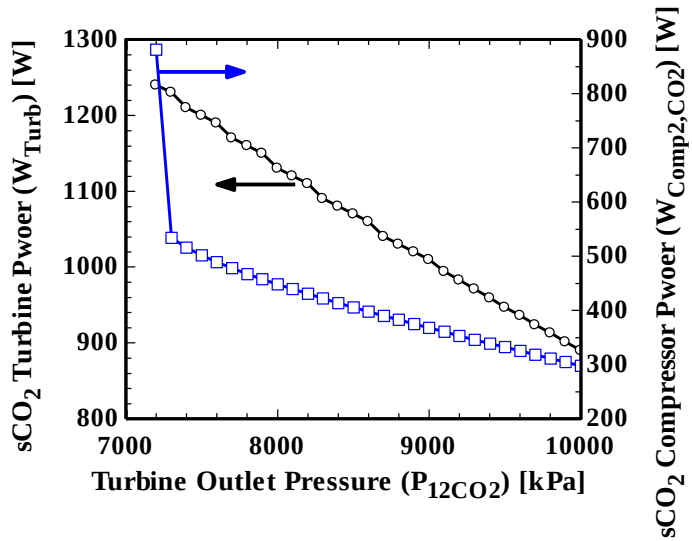

Fig. 15. Turbine power (W_{Turb}) and compressor power ($W_{Comp2,CO2}$) variation with turbine outlet pressure (P_{12CO2}).

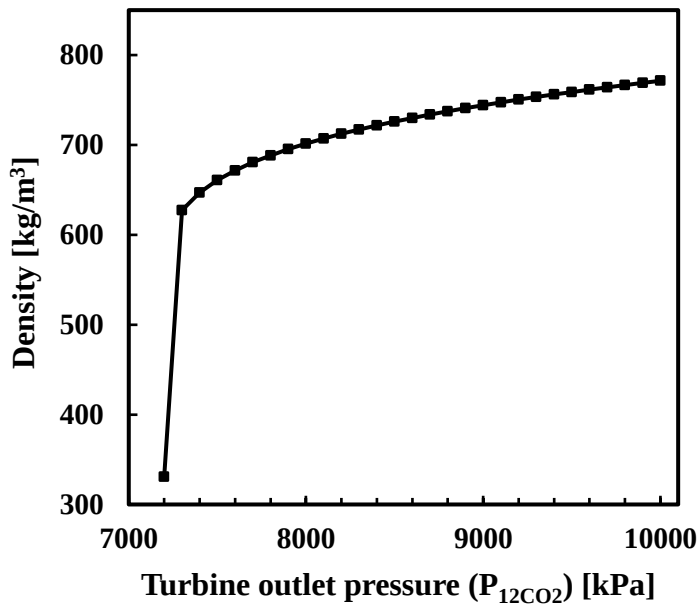

Fig. 16. Compressor inlet density variation with turbine outlet pressure (P_{12CO2}).

The progress of the CO_2 through the HP and sCO_2 cycle to the final state $14CO_2$ is revealed in the P-h diagram in Fig. 17. For each intercooling stage, a certain amount of heat is recovered while that remaining is ejected into the environment. A simple sCO_2 rather the recuperative sCO_2 cycle is integrated to generate power, due to a low outlet temperature of the turbine (T_{12CO2}).

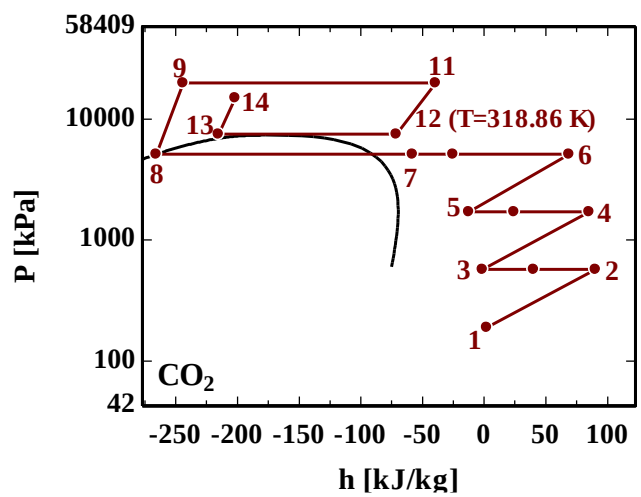

Fig. 17. Pathway of CO_2 in the proposed pressurization process.

The integrated sCO_2 cycle generates a net power of 982.61 kW, with a cycle efficiency (η_{Cycle}) of 9.01% and a heat source temperature around 400 K. Furthermore, the new design utilized the CO_2 prior to storage, with no additional working fluid inventory required to operate the cycle. Table 8 summarizes the state of CO_2 and R290, with the HP installed after the third stage.

Table 8. State properties of CO_2 and R290 in the proposed pressurization process.

State	Fluid	Temperature [K]	Pressure [kPa]	Enthalpy [kJ/kg]
$1CO_2$	CO_2	303.16	190	2.54
$2CO_2$	CO_2	402.45	570	90.46
$3CO_2^{/}$	CO_2	348.74	570	40.17
$3CO_2$	CO_2	303.16	570	-0.95
$4CO_2$	CO_2	403.03	1710	85.27
$5CO_2^{/}$	CO_2	340.74	1710	24.47
$5CO_2$	CO_2	303.16	1710	-12.15
$6CO_2$	CO_2	404.51	5130	68.83
$7CO_2^{/}$	CO_2	324.74	5130	-25.01
$7CO_2$	CO_2	303.16	5130	-57.65
$8CO_2$	CO_2	288.50	5130	-265.75
$9CO_2$	CO_2	306.74	20000	-244.00
$9CO_2^{/}$	CO_2	306.74	20000	-244.00
$9CO_2^{//}$	CO_2	306.74	20000	-244.00
$10CO_2$	CO_2	394.14	20000	-35.47
$10CO_2^{/}$	CO_2	391.21	20000	-41.31
$10CO_2^{//}$	CO_2	390.47	20000	-42.80
$11CO_2$	CO_2	392.33	20000	-39.06
$12CO_2$	CO_2	318.87	7500	-71.04
$13CO_2$	CO_2	303.16	7500	-215.00
$14CO_2$	CO_2	320.17	15000	-201.70
1Refr	R290	288.50	642.91	595.3
2Refr	R290	313.17	1079.26	626.6
3Refr	R290	303.16	1079.26	279.4
4Refr	R290	283.50	642.91	279.4

4. Performance comparison based on equivalent work:

After optimizing the capture and pressurization process, the $W_{Eq,PC}$ is calculated using Eq. (8). Table 9 summarizes the power consumptions of the base and proposed case, as well as the ϕ_{Net}. The performance of the proposed system is reported at the optimized conditions. As Table 9 shows, the new design successfully reduces the boiler duty from 3.36 to 2.65 GJ/TonneCO_2. The modifications to the capture process include optimizing the split ratio in the splitter, adding a heat exchanger as the stripper inter-heater and adding a compressor for the HP. The optimization of the split ratio reduces the reboiler's

heat duty by achieving a better thermal match within the overhead heat exchanger and the economizer. For the stripper inter-heater, the condensate from the reboiler served as the heating utility and no additional heat source was required. The new capture process design involves an additional compressor in the HP, as discussed in section 3.1.2, which results in an additional electric power consumption of 1112 kW. The detailed thermodynamic state properties of the complete proposed system are provided in the supplementary material (Appendix A and B).

The electric power requirement for CO_2 pressurization was reduced from 16691 to 14708 kW using the sCO_2 cycle-integrated HP liquefaction and pressurization system. The proposed CCS design results in a significant saving of ϕ_{Net} = 15.8% in equivalent work. The ϕ_{Net} shows the unified impact of heat and electric power, while the individual saving on the heat duty and electric power is 21.1% and 5.22%, respectively. This study is concerned with minimizing energy expenditure for the CCS process, which improves the prospects of CCS systems being deployed in the power plant sector. However, the reduction in energy consumption is achieved by adding a heat exchanger and a compressor to the capture process and assisting the compression chain with a HP refrigeration cycle and sCO_2 cycle. The proposed pressurization system has the advantage of reducing a CO_2 compressor stage, however, it involves an additional HP and sCO_2 cycle footprint. To quantify the economic behavior of the proposed system would require detailed cost modeling of the capture process, the CO_2 compression chain and HP system components. The current paper focuses on the energy expenditure of the proposed system, while the future outlook entails an economic assessment of the proposed design.

Table 9. Performance indicators of the base and the proposed system.

	Reboiler Heat Duty [GJ/Tonne CO_2]	**Electric Power in Capture Process [kW]**	**CO_2 Compre-ssion [kW]**	**CO_2 Pump [kW]**	**HP Compressor [kW]**	**sCO_2 Power [kW]**	**Equival-ent Work**
Baseline Case (BC)	3.36	N/A	16691	N/A	N/A	N/A	0.974
Proposed Case (PC)	2.65	1112	13465	1149	1077	983	0.820

5. Conclusion

This study designed and evaluated a novel carbon capture and storage process configuration. The proposed configuration successfully reduced the energy expenditure of the carbon capture and storage

process by enhancing heat integration. During the capture process, effective heat integration was achieved by incorporating three stripper modifications, namely: lean vapor compression, rich solvent splitting with vapor heat recovery and reboiler condensate heat recovery using an inter-heater stripper in a single flowsheet. The power required for the CO_2 pressurization was reduced by assisting the multistage compressors with a heat pump system. The multistage compressors then increased then CO_2 pressure to the level needed for liquefaction. The CO_2 was then liquefied in the heat pump system and subsequently pumped to the required pressure. To improve the CO_2 pressurization process, intercooling heat lost during multistage compression was recovered by integrating the heat pump-assisted pressurization scheme with a supercritical CO_2 power cycle.

The performance of the proposed configuration was evaluated for a range of key operating parameters, i.e. split fraction (from 0.65 to 0.74), flash pressure (from 1.0 to 1.6 bar), stripper inter-heater location (from 2 to 18 stages) and flow rate (1000 to 3000 kmol/hr), as well as CO_2 liquefaction pressure (1710 and 5130 kPa), and the low pressure level of the supercritical CO_2 cycle (from 70 to 100 bar). The parametric investigation results indicated the energy expenditure of the proposed configuration was minimized at the optimum values of the split fraction, flash pressure, stripper inter-heater location, stripper inter-heater flow rate, CO_2 liquefaction pressure, and pressure ratio across supercritical CO_2 cycle turbine. The performance of the proposed configuration at the optimized conditions was quantified in terms of equivalent work and it was concluded that 15.8% saving in equivalent work compared to the conventional carbon capture and storage process was achieved using the proposed process configuration. The proposed process configuration demonstrates technical superiority by significantly reducing the energy consumption of both the sequestration and pressurization processes. However, this study has focused on the potential energy savings without considering the capital costs of the proposed modifications, which should be taken into account to ascertain the economic viability of the proposed design.

Acknowledgement

This work was supported by the Development Program of the Korea Institute of Energy Research (KIER B9-2432) and by the "Local Demand Customized R&D Support Project" (Project: Recycling of greenhouse and by-products gases utilizing low-grade waste heat from industrial complex) through the Korea Institute of S&T Evaluation and Planning (KISTEP) funded by the Ministry of Science and ICT, Republic of Korea.

References

1. Energy Information Administration U. International Energy Outlook 2016. 2040.
2. Kılkış Ş, Krajačić G, Duić N, Montorsi L, Wang Q, Rosen MA. Research frontiers in sustainable development of energy, water and environment systems in a time of climate crisis. Energy Conv and Management 2019;199: 111938. https://doi.org/10.1016/j.enconman.2019.111938
3. Singh B, Strømman AH, Hertwich EG. Comparative life cycle environmental assessment of CCS technologies. Int J Greenh Gas Control 2011;5:911–21. doi:10.1016/j.ijggc.2011.03.012.
4. Alami AH, Hawili AA, Tawalbeh M, et al. Materials and logistics for carbon dioxide capture, storage and utilization. Science of The Total Environment 2020;717:137221. https://doi.org/10.1016/j.scitotenv.2020.137221
5. Mikulčić H, Skov IR, Dominković DF, Alwi SR, Manan ZA, Tan R, Duić N, Mohamad SN, Wang X. Flexible Carbon Capture and Utilization technologies in future energy systems and the utilization pathways of captured CO2. Renewable and Sustainable Energy Reviews. 2019 Oct 1;114:109338.
6. Cormos CC. Integrated assessment of IGCC power generation technology with carbon capture and storage (CCS). Energy 2012;42:434–45. doi:10.1016/j.energy.2012.03.025.
7. Leeson D, Mac Dowell N, Shah N, Petit C, Fennell PS. A Techno-economic analysis and systematic review of carbon capture and storage (CCS) applied to the iron and steel, cement, oil refining and pulp and paper industries, as well as other high purity sources. Int J Greenh Gas Control 2017;61:71–84. doi:10.1016/j.ijggc.2017.03.020.
8. Zhao R, Deng S, Zhao L, Liu Y, Tan Y. Energy-saving pathway exploration of CCS integrated with solar energy: literature research and comparative analysis. Energy Conversion and Management. 2015 Sep 15;102:66-80.
9. Barzagli F, Di Vaira M, Mani F, Peruzzini M. Improved solvent formulations for efficient CO_2 absorption and low-temperature desorption. Chem Sus Chem 2012;5:1724–31. doi:10.1002/cssc.201200062.
10. Li K, Leigh W, Feron P, Yu H, Tade M. Systematic study of aqueous monoethanolamine (MEA)-based CO_2 capture process: Techno-economic assessment of the MEA process and its improvements. Appl Energy 2016;165:648–59. doi:10.1016/j.apenergy.2015.12.109.
11. Rezazadeh F, Gale WF, Rochelle GT, Sachde D. Effectiveness of absorber intercooling for CO_2 absorption from natural gas fired flue gases using monoethanolamine solvent. Int J Greenh Gas Control 2017;58:246–55. doi:10.1016/j.ijggc.2017.01.016.
12. Karimi M, Hillestad M, Svendsen HF. Positive and negative effects on energy consumption by interheating of stripper in CO_2 capture plant. Energy Procedia 2012;23:15–22. doi:10.1016/j.egypro.2012.06.066.

13. Cousins A, Cottrell A, Lawson A, Huang S, Feron PHM. Model verification and evaluation of the rich-split process modification at an Australian-based post combustion CO_2 capture pilot plant. Greenh Gases Sci Technol 2012;2:329–45. doi:10.1002/ghg.1295.
14. Gao H, Zhou L, Liang Z, Idem RO, Fu K, Sema T, et al. Comparative studies of heat duty and total equivalent work of a new heat pump distillation with split flow process, conventional split flow process, and conventional baseline process for CO_2 capture using monoethanolamine. Int J Greenh Gas Control 2014;24:87–97. doi:10.1016/J.IJGGC.2014.03.001.
15. Damartzis T, Papadopoulos AI, Seferlis P. Process flowsheet design optimization for various amine-based solvents in post-combustion CO_2 capture plants. J Clean Prod 2016;111:204–16. doi:10.1016/J.JCLEPRO.2015.04.129.
16. Le Moullec Y, Neveux T, Al Azki A, Chikukwa A, Hoff KA. Process modifications for solvent-based post-combustion CO_2 capture. Int J Greenh Gas Control 2014;31:96–112. doi:10.1016/J.IJGGC.2014.09.024.
17. Haider Sultan, Umair H. Bhatti, Jin Soo Cho. Minimization of Energy Consumption for Amine Based CO_2 Capture Process by Process Modification. Journal of Energy Engineering, 2019;28(4):13–18. https://doi.org/10.5855/ENERGY.2019.28.4.013
18. Aminu MD, Nabavi SA, Rochelle CA, Manovic V. A review of developments in carbon dioxide storage. Appl Energy 2017;208:1389-1419. https://doi.org/10.1016/j.apenergy.2017.09.015.
19. Moore JJ, Lerche A, Delgado H, Allison T, and Pacheco J. Development of advanced centrifugal compressors and pumps for carbon capture and sequestration applications. In: Proceedings of the Fortieth Turbomachinery Symposium 2011.
20. Witkowski A, Rusin A, Majkut M, Rulik S, Stolecka K. Comprehensive analysis of pipeline transportation systems for CO_2 sequestration. Thermodynamics and safety problems. Energy Conv and Management 2013;76:665-673. https://doi.org/10.1016/j.enconman.2013.07.087.
21. Moore JJ, Nored MG. Novel concepts for the compression of large volumes of carbon dioxide. In: Proceedings of ASME turbo expo 2008.
22. Alabdulkarem A, Hwang Y, Radermacher R. Development of CO_2 liquefaction cycles for CO_2 sequestration. Appl Thermal Engineering 2012;33(34):144-156. https://doi.org/10.1016/j.applthermaleng.2011.09.027.
23. Romeo LM, Bolea I, Lara Y, Escosa JM. Optimization of intercooling compression in CO_2 capture systems. Appl Thermal Engineering 2009;29:1744-51. https://doi.org/10.1016/j.applthermaleng.2008.08.010.

24. Kurtulus K, Coskun A, Ameen S, Yilmaz C, Bolatturk A. Thermoeconomic analysis of a CO_2 compression system using waste heat into the regenerative organic Rankine Cycle. Energy Conv and Management 2018;168:588-598. https://doi.org/10.1016/j.enconman.2018.05.037.
25. Pei P, Barse K, Gil AJ, Nasah J. Waste heat recovery in CO_2 compression, Int J Greenh Gas Control 2014;30:86–96. https://doi.org/10.1016/j.ijggc.2014.09.001.
26. Farajollahi H, Hossainpour S. Application of organic Rankine cycle in integration of thermal power plant with post-combustion CO_2 capture and compression. Energy 2017;118:927-36. https://doi.org/10.1016/j.energy.2016.10.124.
27. Xu C, Xin T, Li X, Li S, Sun Y, Liu W, Yang Y. A thermodynamic analysis of a solar hybrid coal-based direct-fired supercritical carbon dioxide power cycle. Energy Conv and Management. 2019 Sep 15;196:77-91.
28. Ghorbani B, Mehrpooya M, Omid E. Hybrid solar liquefied natural gas, post combustion carbon dioxide capture and liquefaction. Energy Conv and Management 2020;207:112512. https://doi.org/10.1016/j.enconman.2020.112512
29. Muhammad H.A., Roh C., Cho J., Rehman Z., Sultan H., Baik Y.J., Lee B.J., A comprehensive thermodynamic performance assessment of CO2 liquefaction and pressurization system using a heat pump for Carbon Capture and Storage (CCS) process. Energy Conversion and Management 2020; 206:112489.
30. Aliyon K, Hajinezhad A, Mehrpooya M. Energy assessment of coal-fired steam power plant, carbon capture, and carbon liquefaction process chain as a whole. Energy Conversion and Management. 2019 Nov 1;199:111994.
31. Jin H, Liu P, Li Z. Energy-efficient process intensification for post-combustion CO_2 capture: A modeling approach. Energy 2018;158:471–83. doi:10.1016/J.ENERGY.2018.06.045.
32. Sarkar J. Review and future trends of supercritical CO_2 Rankine cycle for low-grade heat conversion. Renewable and Sustainable Energy Reviews 2015;48:434-451. https://doi.org/10.1016/j.rser.2015.04.039.
33. Liu Y, Zhang L, Watanasiri S. Representing Vapor−Liquid Equilibrium for an Aqueous MEA− CO_2 System Using the Electrolyte Non Random-Two-Liquid Model. Ind Eng Chem 1999;38(5):2080-2090. doi:10.1021/IE980600V.
34. Le Moullec Y, Kanniche M. Screening of flowsheet modifications for an efficient monoethanolamine (MEA) based post-combustion CO_2 capture. International journal of greenhouse gas control 2011;5(4):727-740.
35. Takenouchi S, Kennedy GC. The binary system H_2O-CO_2 at high temperatures and pressures. American Journal of Science 1964;262:1055–74. doi:10.2475/ajs.262.9.1055.

36. Wang YW, Xu S, Otto FD, Mather AE. Solubility of N_2O in alkanolamines and in mixed solvents. The Chem Engg Journal 1992;48(1):31–40. doi.org/10.1016/0300-9467(92)85004-S.
37. Austgen DM, Rochelle GT, Peng X, Chen CC. Model of vapor-liquid equilibria for aqueous acid gas-alkanolamine systems using the electrolyte-NRTL equation. Ind Eng Chem Res 1989;28:1060–73. doi:10.1021/ie00091a028.
38. Bravo LJ. Mass Transfer in Gauze Packings. Hydrocarb Process 1985;64:91–5.
39. Muhammad HA, Lee B, Lee G, Cho J, Baik YJ. Investigation of leakage reinjection system for supercritical CO_2 power cycle using heat pump. Renewable Energy 2019;144:97-106. https://doi.org/10.1016/j.renene.2018.10.059.
40. Campos JC, Moura D, Costa AP, Yokoyama L, Araujo FV, Cammarota MC, Cardillo L. Evaluation of pH, alkalinity and temperature during air stripping process for ammonia removal from landfill leachate. Journal of Environmental Science and Health, Part A 2013;48(9):1105-13.
41. Zhao Y, Wang B, Chi J, Xiao Y. Parametric study of a direct-fired supercritical carbon dioxide power cycle coupled to coal gasification process. Energy Conv and Management 2018;156:733-745. https://doi.org/10.1016/j.enconman.2017.11.044